EARTHQUAKE ENGINEERING AND STRUCTURAL DYNAMICS
Earthquake Engng Struct. Dyn. 2010; **00**:1–20
Published online in Wiley InterScience (www.interscience.wiley.com). DOI: 10.1002/eqe

High-resolution seismic monitoring of instrumented buildings using model-based state observers

K. Erazo[‡] and E. M. Hernandez[*†]

School of Engineering, College of Engineering and Mathematical Sciences, University of Vermont, VT, USA

SUMMARY

This paper proposes a model-based state observer to perform high-definition response estimation in partially instrumented building structures. The proposed estimator is verified in a 5-story simulated shear-building structure and validated using measurements from a 7-story reinforced concrete building slice tested at the NEES-UCSD shake table. In both cases the proposed estimator yielded satisfactory results by estimating the time history of shear forces, bending moments, displacements and strains at various locations of interest. The proposed algorithm can be used in instrumented buildings for various practical applications, including post-earthquake damage assessment, structural control and building codes calibration.

Received . . .

KEY WORDS: seismic response estimation, vibration measurements, state observers, experimental validation, estimation

1. INTRODUCTION

The analysis of vibration signals measured in building structures during earthquakes provides useful information that can help engineers to enhance the accuracy of building models [1, 2], improve seismic code provisions [3], and to perform post-earthquake damage assessment [4, 5, 6]. Due to economic and/or logistical constraints, strong motion instrumentation in buildings typically consists of absolute acceleration measurements at the base, the roof, and at a limited number of intermediate stories. The number and location of accelerometers depends on the height and complexity of the building. Due to this limitation, not all quantities of interest (QoI) such as internal forces, drifts and strains (among others) can be directly measured.

Various levels of spatio-temporal resolution for structural monitoring and response estimation of instrumented buildings can be established. These range from tracking changes in vibration frequencies before, during and after the potentially damaging seismic event, to tracking the complete dynamic response and model parameters during the event at a measurement rate (typically around 100Hz). This paper deals with high-definition spatio-temporal tracking of QoI such as internal forces, displacement and strain fields throughout the elements of the building structure at the measurement sampling rate.

In the case of low seismic demands, linear interpolation has been proposed by various researchers to perform response estimation. Early work carried out by Mau and Aruna [7] used mode shapes as interpolating functions to estimate the one-dimensional displacement and interstory drift response

[*]Correspondence to: School of Engineering, 33 Colchester Ave, Burlington, VT.
[‡]E-mail: kalil.erazo@rice.edu
[†]E-mail: eric.hernandez@uvm.edu

at unmeasured stories. Interstory shear forces and overturning moments were computed using story weight information gathered from building drawings and the interpolated accelerations (neglecting the effect of damping). More recently, Limongelli [8] used more general spline functions to interpolate the seismic response in buildings. Some challenges typically encountered when using interpolation methods are: (i) the user needs to decide which interpolating functions to use; if mode shapes are used, the modes need to be specified (usually the lower frequency modes are selected, however in tall buildings this is not always the best choice [9]); (ii) The interpolation approach is static, and as such, the estimated response at time t only depends on the measurements at time t; (iii) if n sensors are used, then the interpolation approach only allows the use of, at most, n independent interpolating functions. Finally, under strong motions the modal interpolation is expected to fail, since the building response is no longer characterized by a linear superposition of modal responses.

Recently, methods based on response feedback and state observers have been proposed to perform estimation of unmeasured seismic response in instrumented building structures [9]. This paper proposes the use of a finite element model-based state observer recently developed by one of the authors to estimate the complete temporal and spatial response of the internal forces, displacements, strain and stress fields at a high resolution level [10].

The proposed model-based observer is verified in the context of a simulated five degree-of-freedom nonlinear shear model and validated using results of a full-scale experiment performed by an independent team of researchers from the University of California at San Diego (UCSD). The experiment consisted of a seven story reinforced concrete building slice tested on the NEES-UCSD shake table [11]. The NEES-UCSD test structure was densely instrumented and progressively subjected to synthetic broadband noise excitations and historical ground motions. A detailed description of the instrumentation and testing program can be found in Panagiotou et al. [11]. The measured data has been successfully employed by other researchers to validate system and damage identification techniques [12, 13]. To the best knowledge of the authors, this paper constitutes the first attempt to use an experiment of this size and complexity to validate state observers in seismic response estimation applications.

2. STATE ESTIMATION IN STRUCTURAL SYSTEMS

2.1. Systems of Interest

The systems of interest are building structures subjected to seismic ground motions. The dynamic response of these systems can be approximately modeled by a set of simultaneous differential equations of the form

$$\mathbf{M}\ddot{q}(t) + \mathbf{C}_d\dot{q}(t) + f_R(q(t), z(t)) = \mathbf{B}_1\ddot{u}_g(t) + w(t) \tag{1}$$

where $q(t) \in \mathbb{R}^N$ is the displacement vector (relative to the ground motion), $z(t)$ is a vector of auxiliary variables dealing with material nonlinear and damage behavior, N is the number of degrees-of-freedom (DOF), $\mathbf{M} \in \mathbb{R}^{N\times N}$ is the mass matrix, $\mathbf{C}_d \in \mathbb{R}^{N\times N}$ is the damping matrix and $f_R(\cdot)$ is the static restoring force function. The matrix $\mathbf{B}_1 = -\mathbf{M}r$ where r is the ground motion influence vector. The vector $w(t) \in \mathbb{R}^N$ is the process noise used to model unmeasured inputs, measurement noise in measured inputs and/or modeling errors.

Absolute acceleration response measurements are modeled as

$$y(t) = \mathbf{c}_2\mathbf{M}^{-1}\left[w(t) - \mathbf{C}_d\dot{q}(t) - f_R(q(t), \dot{q}(t))\right] + \nu(t) \tag{2}$$

where $\mathbf{c}_2$ is a Boolean matrix indicating the measured degrees of freedom and $\nu(t)$ represents the measurement noise, which in this paper will be modeled as an independent Gaussian process with zero mean and covariance $\mathbf{R}$. In practice, the measurements are digital and thus measurements are only available at times that are multiple of the inverse of the sampling rate.

DOI: 10.1002/eqe

2.2. State Estimation in Structural Dynamics

The term *state* refers to the minimum number of response quantities at a given time t_o necessary to predict the future response of the system ($t > t_o$) in the absence of external excitations. In the case of linear structural systems with velocity proportional damping, the state consists of displacement and velocity at all degrees of freedom. For nonlinear systems, the state may also include auxiliary response quantities that describe the evolution of the restoring force function.

State estimation refers to a collection of algorithms that use noise-contaminated measurements of a system response in a feedback loop to estimate (or track) the complete state of the system. The resulting feedback system is known as a state observer [14, 15]. The fundamental component of all state observers is the feedback gain, i.e., the matrix that weighs the effect of the measurements in the feedback loop.

State observers are common in control systems and have had limited application in structural dynamics [16]. Recent application of state estimation with emphasis in reconstructing seismic response of buildings can be found in [17, 9, 18]. In [17] a particle filter was used to estimate the complete lateral response of a building using vibration data obtained during the Northridge earthquake. It was concluded that model error plays an important role and robustness is a mayor issue in state estimation. Due to the large computational cost of implementation (the particle filter is a stochastic simulation filtering method), it was necessary to use a relatively simple model which had a detrimental effect on the estimation quality. In [9] a robust linear state observer was proposed and tested using real data from instrumented buildings. Although satisfactory results were obtained for linear response, the robust observer did not fully account for the effects of measurement noise and unmeasured excitation. In addition it requires measurement of the excitation and a relatively low order model in order to be implemented efficiently. More recently, in [18], various nonlinear Bayesian state estimation methods were compared. Specifically, the extended, unscented, ensemble Kalman filter and the particle filter were implemented for seismic response reconstruction. Sensitivity to nonlinear behavior and robustness to various types of model error were considered in the context of simulated buildings. It was found that all filters exhibit significant sensitivity to model error (in agreement with the results obtained by Ching et al. [17]). It was found that the unscented Kalman filter was the most efficient of the methods considered.

In order to address some of the existing scalability and robustness limitations of traditional state estimators, this paper proposes the use of a recently developed finite element model-based observer [10]. The observer was originally proposed for symmetric second-order systems, and this paper presents its first application in the context of seismic response reconstruction. The proposed observer has several advantages over existing state estimators. First, it was originally formulated such that it can be efficiently implemented in the context of a finite element model. Instead of operating in state-space (first-order form), the proposed observer operates directly in second-order form; this significantly reduces the computational cost of implementation [19].

Moreover, the formulation of the observer allows for the use of high-order and detailed finite element (FE) models, which results in increased resolution and accuracy. Other advantages are: The observer is natural, meaning that the estimates of velocity are actually derivatives of the displacement estimates. This is not the case with other linear estimators, such as the Kalman filter [10]. The observer is slightly suboptimal, which implies that its sensitivity to modeling errors is reduced. In the context of this paper the Kalman filter is considered to be the optimal estimator, in the sense that it minimizes the trace of the state error covariance matrix. As discussed in the following section, the proposed observer minimizes only the displacement component of the state error covariance matrix, and for this reason is considered a suboptimal estimator. The proposed observer has been found effective in the context of small scale laboratory experiments [19]. This paper aims to test its effectiveness in the context of a large-scale test setup were modeling errors are likely to play an important role, and a refined finite element model is necessary to obtain satisfactory estimation results.

DOI: 10.1002/eqe

2.3. Finite Element Model-Based Observer

The finite element model-based observer (MBO) is a recently developed state observer for second-order symmetric systems [10]. In the MBO the estimate of the displacement response of the structure, $\hat{q}$, is given by the solution of

$$\mathbf{M}\ddot{\hat{q}}(t) + (\mathbf{C}_D + \mathbf{c}_2^T\mathbf{E}\mathbf{c}_2)\dot{\hat{q}}(t) + \mathbf{K}\hat{q}(t) = \mathbf{c}_2^T\mathbf{E}\dot{q}_m(t) = f_c(t) \tag{3}$$

where $\dot{q}_m$ is the measured velocity (readily obtained from acceleration measurements), and $\mathbf{E} \in \mathbb{R}^{m\times m}$ is the feedback gain. A physical interpretation of the MBO can be obtained by interpreting the right-hand side of Equation 3 as a set of corrective forces that act on a modified version of the original model. The corrective forces result from enforcing the constraint that the observer can be implemented as a finite element model [10]. The modification to the model consists in adding the damping term $c_2^T\mathbf{E}c_2$. In order to retain a physical interpretation, $c_2^T\mathbf{E}c_2$ must be a symmetric and positive semi-definite matrix. .

To determine $\mathbf{E}$ the objective function to be minimized in the MBO is the trace of the displacement error covariance matrix, given by

$$J = tr(\mathbb{E}[(q(t) - \hat{q}(t))(q(t) - \hat{q}(t))^T]) = tr\left(\int_{-\infty}^{+\infty} \Phi_{ee}(\omega)d\omega\right) \tag{4}$$

where the estimation error power spectral density matrix Φ_{ee} is

$$\Phi_{ee} = \mathbf{H}_o\mathbf{b}_2\Phi_{ww}\mathbf{b}_2^T\mathbf{H}_o^* + \mathbf{H}_o\mathbf{c}_2^T\mathbf{E}\Phi_{vv}\mathbf{E}^T\mathbf{c}_2\mathbf{H}_o^* \tag{5}$$

with $\mathbf{H}_o$ defined as

$$\mathbf{H}_o = \left(-\mathbf{M}\omega^2 + \left(\mathbf{C}_D + \mathbf{c}_2^T\mathbf{E}\mathbf{c}_2\right)i\omega + \mathbf{K}\right)^{-1} \tag{6}$$

The matrices Φ_{ww} and Φ_{vv} are, respectively, the power spectral density of the uncertain inputs and measurement noise. In this paper the uncertain input corresponds to the ground motion excitation and the measurement noise corresponds to the accelerometer measurement errors. A detailed derivation of the MBO can be found in [10, 19].

3. NUMERICAL VERIFICATION

In this section the MBO is numerically verified in a simulation environment, in the context of a five degree-of-freedom nonlinear shear building model subjected to a moderate support motion. A nonlinear Bouc-Wen-Baber-Noori model with strength/stiffness degradation was adopted to model the system [20, 21]. In this model the internal spring forces are given by

$$f_r(q(t), \dot{q}(t), z(t); \theta) = akq(t) + (1-a)Dkz(t) \tag{7}$$

$$\dot{z}(t) = (\eta(t)D)^{-1}\left[A(t)\dot{q}(t) - \nu(t)\beta z(t)|\dot{q}(t)||z(t)|^{n-1} - \nu(t)\gamma\dot{q}(t)|z(t)|^n\right] \tag{8}$$

where $z(t)$ is the normalized hysteretic force, k is the initial stiffness, D the yield displacement, a is the ratio of post-yield and pre-yield stiffness, $\{\gamma, \beta\}$ control the shape of hysteresis loops, and n governs the smoothness of the transition from elastic to plastic response. The function $\nu = 1 + \delta_\nu D_E$ controls the strength degradation between hysteresis loops, $\eta = 1 + \delta_\eta D_E$ controls the stiffness degradation between hysteresis loops, and $A = 1 + \delta_A D_E$ controls the continuous stiffness/strength degradation during hysteresis cycles. D_E denotes the hysteretic dissipated energy.

The following parameters were used as nominal values: $k_n = 4\pi^2 N/m$, $D_n = 0.25m$, $\gamma = 0.8$, $\beta = 0.2$, and $\nu = 2$. The mass was $M = 1kg$ and a damping ratio of 5% in all modes. The fundamental vibration frequency of the model was 2Hz. The degradation parameters were chosen as $\delta_\nu = 1 \times 10^{-5}1/Nm$, $\delta_\eta = 1 \times 10^{-5}1/Nm$ and $\delta_A = 1 \times 10^{-6}1/Nm$ [22]. The parameters and

DOI: 10.1002/eqe

the level of nonlinearity in this numerical example were selected based on the experimental results of the following section, which constitute the main contribution of this paper.

To model seismic ground motion the Kanai-Tajimi stochastic process was adopted [23]. In this model ground motions are given by

$$u(t) = I(t)\left[\omega_g^2 u_g(t) + 2\xi_g\omega_g\dot{u}_g(t)\right] \tag{9}$$

where $u_g(t)$ is the solution of

$$\ddot{u}_g(t) + 2\xi_g\omega_g\dot{u}_g(t) + \omega_g^2 u_g(t) = w(t) \tag{10}$$

$w(t)$ is formally a white noise process with spectral density $S_{ww}(\omega) = G_o$, and $I(t)$ is an amplitude modulating function. The process $u^*(t) = u(t)/I(t)$ has a Kanai-Tajimi power spectral density given by

$$S_{u^*u^*}(\omega) = G_o \frac{1 + 4\xi_g^2\left(\frac{\omega}{\omega_g}\right)^2}{\left[1 - \left(\frac{\omega}{\omega_g}\right)^2\right]^2 + 4\xi_g^2\left(\frac{\omega}{\omega_g}\right)^2} \qquad -\infty < \omega < \infty \tag{11}$$

The parameters ξ_g and ω_g of the Kanai-Tajimi model have been extensively calibrated with recorded ground motions (Pires et al. [24], and references therein). Other ground motion models based on filtered white noise can be implemented in a similar way. The parameters values used are $\omega_g = 15rad/s$ and $\xi_g = 0.35$; these values are characteristic of firm soils [24]. The underlying white noise spectral density G_o was found such that a target peak ground acceleration (PGA) of $0.20g$ is obtained in the mean. For this purpose the relationship between the PGA and the root mean square acceleration developed by Vanmarcke and Lai was used [25].

The amplitude modulating function $I(t)$ was selected as

$$I(t) = te^{-bt} \tag{12}$$

where $b = 0.30$ based on calibration results using past seismic records [26].

3.1. Implementation of MBO

To implement the MBO the system was linearized around its position of static rest. The spectral density matrix Φ_{ww} was selected based on the Kanai-Tajimi model given by Equation 11. The measured response consisted of absolute acceleration measurements, contaminated with an additive zero mean white Gaussian sequence with a noise-to-signal RMS (root-mean-square) ratio of 0.10. The measured locations were the second and fifth DOF. The measurement noise spectral density matrix Φ_{vv} was selected based on the RMS noise to signal ratio of 0.10.

As explained in [10], one of the advantages of the MBO is that is can be implemented as a physical system. This observer is a modified version of the system of interest subjected to corrective forces which drive the observer. Any response quantity from the observer (i.e., the modified model) constitutes an estimate of the same quantity in the system of interest. The implementation of the observer is depicted in Figure 1. The system of interest is shown on the left, while the observer system is shown on the right. In this case the modification are dampers at the measurement locations and the corrective forces are the measured velocities scaled by the damper values. The dampers values are obtained in such a way that the sum of the displacement error variances is minimized. This is done by optimizing Equation 4. Results from the optimization are presented in Figure 2. Special care must be taken when integrating Equation 4; the integration was approximated using the trapezoidal rule with a $\Delta\omega = 0.025rad$ and with an upper limit of $\omega_{max} = 1,256rad$, convergence was verified. The damper values $c_1 = 13.98 \times 10^7 Ns/m$ and $c_2 = 13.54 \times 10^7 Ns/m$ minimize the covariance of the state error (J in Equation 4).

Prepared using eqeauth.cls
DOI: 10.1002/eqe

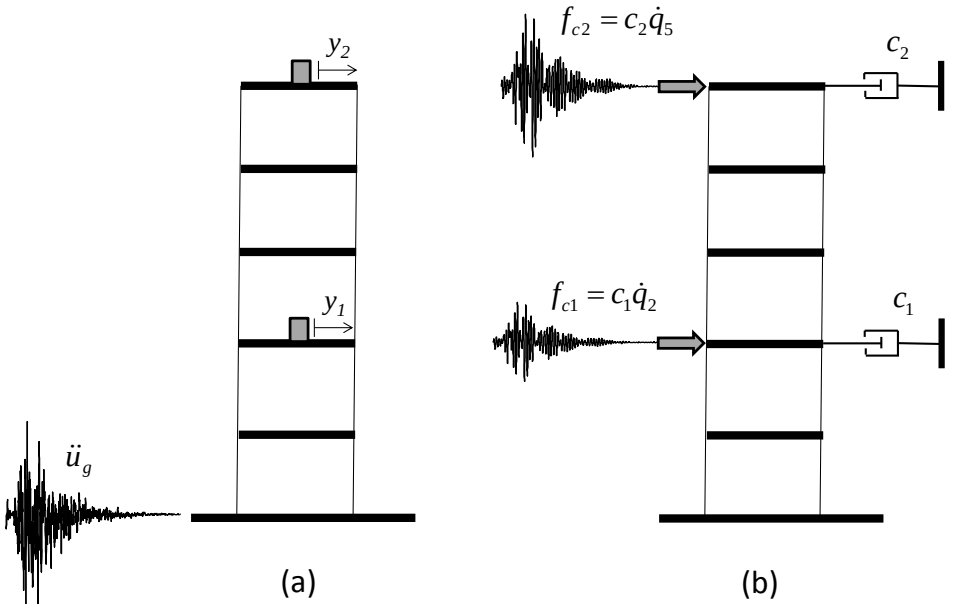

Figure 1. Depiction of the MBO in a 5-degree of freedom shear building subjected to a support motion. (a) The system of interest with support motion and measurements, (b) The MBO with corrective forces.

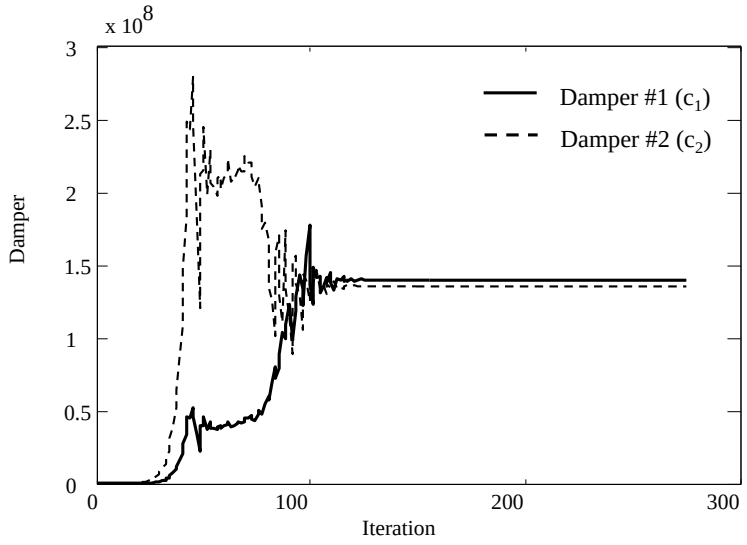

Figure 2. Evolution of the dampers c_1 and c_2 as a function of the number of iterations

DOI: 10.1002/eqe

3.2. Estimation Results

Table I presents a comparison of the estimates given by the observer for the maximum inter-story drifts. The estimates are in close agreement with the system response. Similarly, Table II presents a comparison of the estimates of the maximum inter-story shear force, where again the estimates are consistent with the system response. Figure 3 depicts the time history of the estimates of the lateral displacement of DOF 1 and DOF 4.

Table I. Estimated maximum drift displacement ($\times 10^{-2} m$).

Story	1	2	3	4	5
SYS	1.48	1.38	1.12	0.85	0.46
MBO	1.46	1.36	1.12	0.87	0.47

Although encouraging, these results are under ideal conditions. In these simulations no modeling errors are considered, and the system does not experience large nonlinear excursions. The next section examines an experimental validation on a full-scale slice of a building, where the specimen was subjected to increasing ground motions until significant degradation was observed.

Table II. Estimated maximum inter-story shear ($\times 10^{5} N$).

Method	1	2	3	4	5
SYS	6.25	5.90	5.08	3.80	2.06
MBO	6.65	6.23	5.26	3.89	2.12

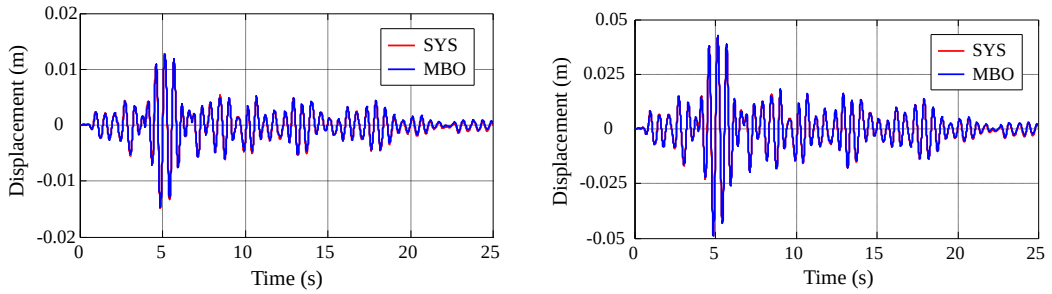

Figure 3. DOF 1 (left) and DOF 4 (right) displacement estimates.

4. EXPERIMENTAL VALIDATION

In this section the performance of the proposed MBO is assessed using vibration data from an experiment performed by a team of researchers from the University of California at San Diego (UCSD). The experiment consisted of a densely instrumented full-scale reinforced concrete shear wall structure tested in the NEES-UCSD shake table [11, 27]. To validate the MBO absolute acceleration response measurements at limited locations are used to estimate quantities of interest (QoI) throughout the structure. The estimated QoI are compared to their corresponding measurement, assumed to be unknown during the estimation process. The QoI include lateral displacement, absolute accelerations, strains at critical locations, base shear and overturning moment.

DOI: 10.1002/eqe

4.1. Test Structure Description

The test structure consisted of a seven story full-scale reinforced concrete cantilever shear wall, resembling a "slice" of a typical shear wall building [27]. The structure was designed using the displacement-based capacity approach resulting in smaller design forces than those that result from current force-based design codes [27, 28].

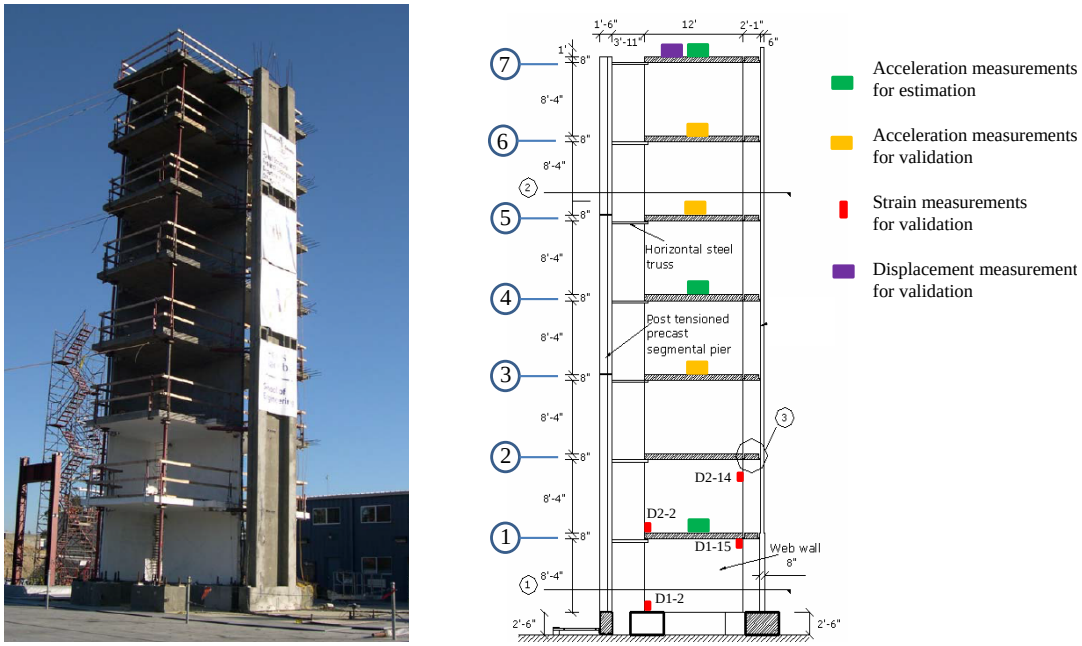

Figure 4. Left: Test structure. Right: Dimensions and sensors used for estimation/validation [11].

The gravity load system consisted of a reinforced concrete slab supported by high-strength columns. The structure was supported by a reinforced concrete foundation, which was connected to the shake table using post-tensioned cables. The test structure on the shake table is shown in the left panel of Figure 4. The structure total height was approximately $20m$. The web wall was $0.30m$ wide, with a thickness of $0.20m$ in levels 1 and 7, and $0.15m$ in levels 2-6. The web wall was connected to a was $5m$ wide flange wall with a thickness of $0.20m$ in level 1 and $0.15m$ in levels 2-7. The web wall was connected to the flange wall using a slotted connection to prevent coupling between the two walls.

On the other end the shear wall was connected to a post-tensioned gravity column by pinned braces (both the column and braces were designed to remain elastic during the test); the purpose of this column was to increase the structure torsional rigidity to reduce out-of-plane effects with respect to the loading direction. The bracing consisted of $100 \times 100 \times 10mm$ angles in levels 1-2, and $75 \times 75 \times 8mm$ angles in levels 3-7.

4.1.1. Instrumentation and Testing Program A dense array of sensors was deployed throughout the structure to measure its dynamics response. The instrumentation included 139 accelerometers, 88 displacement transducers (LVDT), 314 strain gages and 23 pressure transducers sampled at 240 Hz. Additionally an array of 50Hz GPS devices were used to measure lateral displacement response. A total of approximately 600 sensors were used in the experiment [27]. The instrumentation in the first story of the main wall is shown in Figure 5.

The structure was sequentially subjected to four recorded earthquake ground motion time histories: i) the Van Nuys longitudinal component record of 1971 San Fernando earthquake, ii) Van Nuys transverse component record of 1971 San Fernando earthquake, iii) Oxnard Boulevard

DOI: 10.1002/eqe

Figure 5. Web wall first story instrumentation. The top-right corner shows an LVDT in the wall/foundation interface [11].

in Woodland Hill longitudinal component of 1994 Northridge earthquake, and iv) the Sylmar Olive View Med 360 component record from 1994 Northridge earthquake. Before and after each earthquake the structure was subjected to banded (0.25-25 Hz) white noise excitations with varying RMS of 0.02g, 0.03g and 0.05g. In addition, ambient vibration measurements were recorded at the different stages.

4.2. Finite Element Model Used for State Estimation

A three dimensional finite element model of the test structure was developed using the software SAP2000 [29]. The web and flange walls consist of linear elastic shell elements. The web and flange walls are connected using pinned rigid links to model the slotted joint. The precast pier and web wall are joined using end-pinned angles. The model has $11,676$ shell elements and 217 frame elements, with a total number of $73,605$ degrees of freedom. The model is depicted in Figure 6.

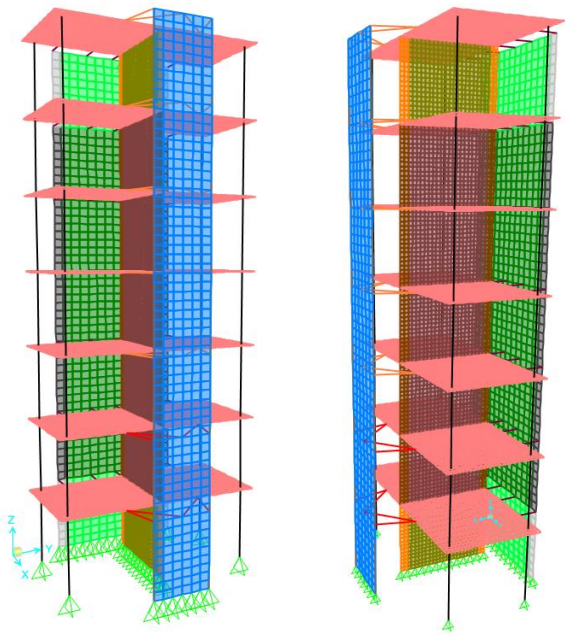

Figure 6. Three dimensional FEM model; the model has $11,676$ shell elements and 217 frame elements, with a total number of $73,605$ degrees of freedom.

DOI: 10.1002/eqe

The material properties were selected as follows: a concrete strength $f'c = 40MPa$ and Young modulus $E_c = 30GPa$; reinforcing steel $Fy = 450GPa$ and $E_s = 200GPa$.

The damping was modeled as Rayleigh such that the first two modes have a damping ratio of 0.025. The damping ratios were selected based on system identification results performed at the beginning of the testing program [13]. The total mass is $216.4 \times 10^3 kg$.

4.3. Reduced Hybrid Model Used to Compute Feedback Gain

In order to perform the gain optimization (Equation 4) in a computationally effective fashion, a reduced model was formulated. The model consists of a close-coupled chain connected to a linear elastic cantilever. Similar models have been proposed to estimate the dynamic response of building structures [30, 31, 32]. The motivation for using this class of models is that the lateral deformation in buildings are in general characterized by a combination of flexural and shear deformations [33]. It has been shown that using only shear-type models may result in significant errors in building response estimates [34, 35]. This has also been shown to be the case in structures in which shear walls are used as the main lateral deformation resisting mechanism [30].

To calibrate the initial stiffness of the model the first three longitudinal vibration frequencies of the finite element model described in the previous section were used. The resulting springs initial stiffness was $k_i = 3.6 \times 10^7 N/m$ and the elastic cantilever $EI = 1 \times 10^{10} Nm^2$. The mass of each DOF in the reduced model corresponds to the tributary mass, i.e., based on half of the mass of the adjacent upper and lower story. The damping matrix is classical with a damping ratio of 0.025 in all modes and kept constant throughout the analyses. The damping ratios were selected based on system identification results performed in Moaveni et al. [13]. The calibrated RHM was used only to perform the gain optimization. To implement the MBO the finite element model presented in Fig. 6 was employed. The use of the refined FEM reduces modeling errors and allows to estimate local quantities such as stress and strains. This last aspect is one of the more attractive features of the MBO.

4.4. Experimental Results

This section presents results of the application of the MBO to estimate the response of the structure during the following tests:

1. Low amplitude banded white-noise (WN); the input consisted of a realization of a $0.02m/s^2$ RMS process with banded power spectral density in the range 0.25-25Hz.
2. Low amplitude earthquake (EQ1); the input consisted of the VNUY longitudinal component of the 1971 San Fernando earthquake (PGA=0.15g).
3. Moderate amplitude earthquake (EQ2); the input consisted of the VNUY transverse of 1971 San Fernando earthquake (PGA=0.26g).

To implement the MBO time histories of acceleration response at the first, fourth and seventh stories were used (see Figure 4). The measured locations were chosen based on the linear observability criteria, i.e., such that the condition number of the observability matrix is minimized [15]. The resulting sensor arrangement is consistent with typical strong motion instrumentation in building structures [5].

The QoI include lateral displacement, lateral accelerations, strains at critical locations, base shear and overturning moment (see Figure 4). The estimated quantities were compared to their corresponding measurements; the QoI measurements were assumed to be unknown during the estimation and only used for validation purposes.

4.4.1. Low amplitude banded white-noise (WN) Estimation results from the application of a white banded (0.25-25Hz) base motion are presented next. The data corresponds to test no. 33 as specified in the testing history [11]. This was one of the initial tests performed, and the structure is thus considered to be in an "uncracked" state. The measurements were sampled at 240Hz, detrended and band-passed (0.5-50Hz) using a high order 1024 FIR filter. The base motion history (measured at the foundation level) is shown in Figure 7, where a zoomed window shows 10 seconds of the input.

DOI: 10.1002/eqe

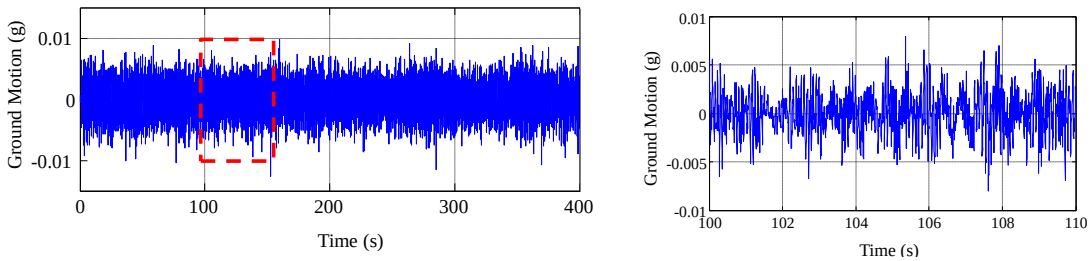

Figure 7. Left: white banded (0.25-25Hz) base motion with an RMS of 0.02g. Right: Zoomed window.

The MBO introduced in the previous section was used to estimate the QoI. The input variance and PSD needed to implement the observer were obtained from an equivalent white noise process [36]. The MBO was implemented using the finite element model introduced in section 4.2. To perform the optimization in Equation 4 the reduced hybrid model was used with the parametrization $\mathbf{E} = E_{ii}\mathbf{I}_{m\times m}$ where $E_{ii} \in [0, \infty)$ and $\mathbf{I}_{m\times m}$ is the m-dimensional identity matrix. A value of $E_{ii} = 1 \times 10^9 Ns/m$ was selected to implement the observer.

The estimate of the strain history at critical locations in the first and second story web wall are presented in Figure 8 and Figure 9 (see Figure 4 for the LVDT layout). As it can be seen, the estimated strains are in good agreement with the corresponding measurements.

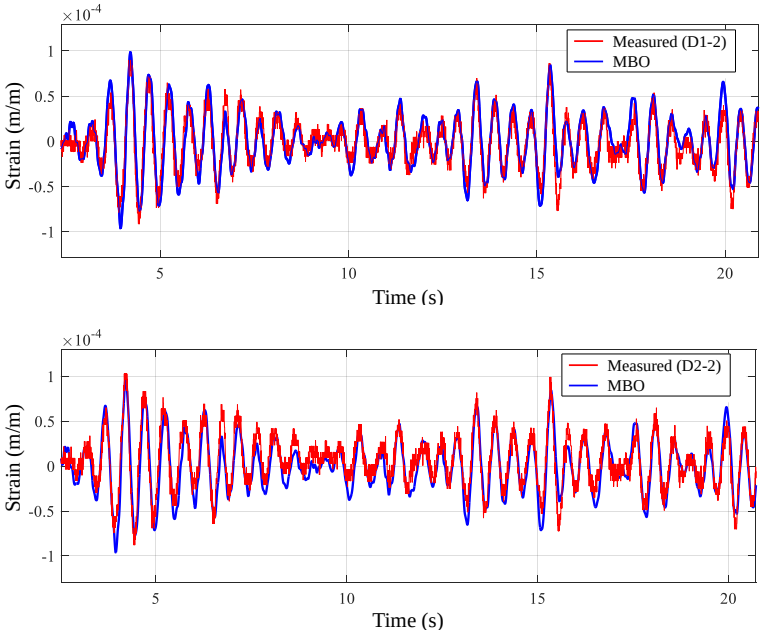

Figure 8. Strain estimates at first story wall (WN test).

DOI: 10.1002/eqe

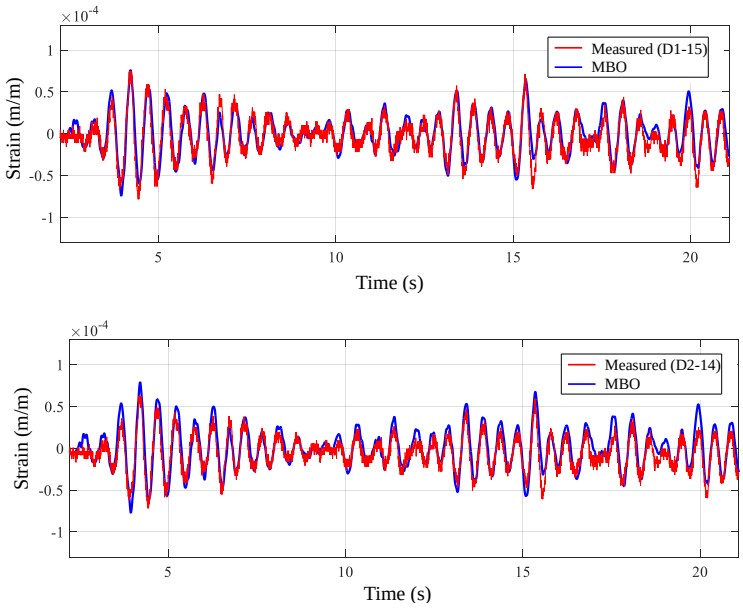

Figure 9. Strain estimates at second story wall (WN test).

4.4.2. Low Amplitude Earthquake Input (EQ1) In the second test a low amplitude base motion was applied to the structure. The applied input was the VNUY longitudinal component of the 1971 San Fernando earthquake (PGA=0.15g), denoted as "EQ1". The base motion corresponds to test no. 93 according to the testing history [11]. The measured acceleration response at the foundation level and the magnitude of its Fourier spectra are presented, respectively, in the upper and lower panels of Figure 10.

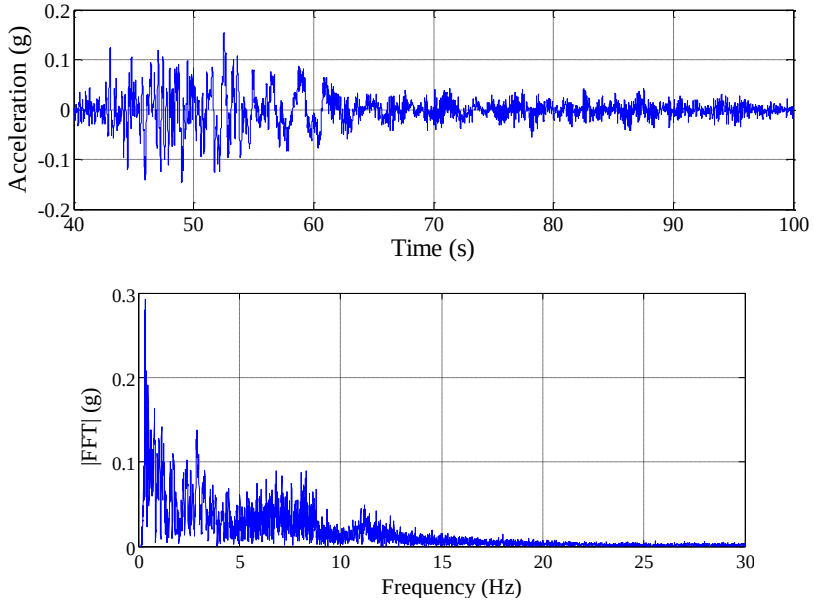

Figure 10. Low Amplitude Earthquake Input (EQ1) - VNUY longitudinal component of the 1971 San Fernando earthquake (PGA=0.15g). Top: Time History. Bottom: Fourier Spectra amplitude.

DOI: 10.1002/eqe

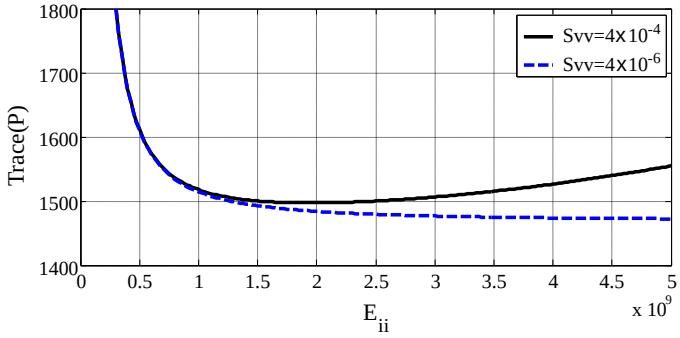

Figure 11. Model-based observer feedback gain optimization.

The MBO was applied to estimate the response of the structure using the same measurements as in the previous case (see Figure 4). The measurements were sampled at 240Hz, detrended and band-passed (0.5-50Hz) using a high order 1024 FIR filter. The correlation in the input was modeled using the Kanai-Tajimi model [37, 38] presented in the verification section (Equations 9 - 12). The parameters were chosen as $w_g = 15rad/s$ and $\xi_g = 0.35$ based on the results in [24]. The white noise input PSD (G_o) was selected such that a PGA of 0.30g is obtained in the mean (recall that the actual input PGA was 0.15g). For this purpose the relationship between the PGA and the root mean square acceleration developed by Vanmarcke and Lai was used [25]. Other input models such as stationary Gaussian white noise and modulated Gaussian white noise were investigated without significant change in the results.

The MBO was implemented using the finite element model introduced in section 4.2. As before, the optimization in Equation 4 was performed using the reduced-hybrid model introduced in section 4.3 with the parametrization $\mathbf{E} = E_{ii}\mathbf{I}_{m\times m}$ where $E_{ii} \in [0, \infty)$ and $\mathbf{I}_{m\times m}$ is the m-dimensional identity matrix. The optimization results are shown in Figure 11. A value of $E_{ii} = 2 \times 10^9 Ns/m$ was selected to implement the filter.

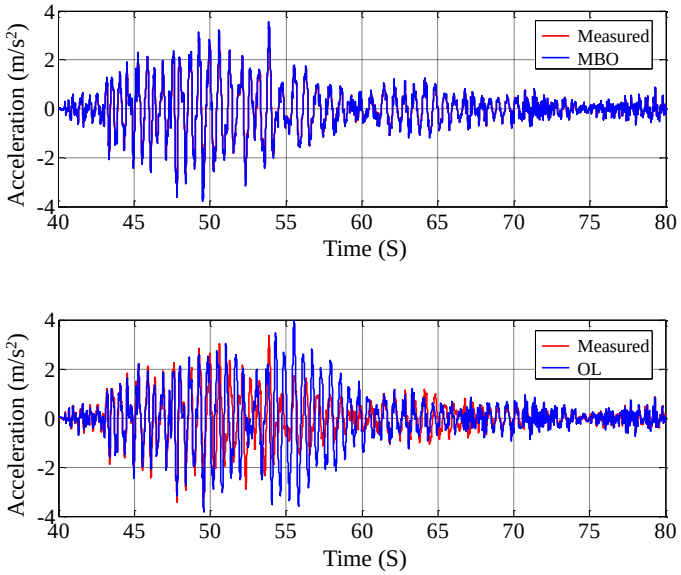

Figure 12. Acceleration estimate at sixth story (EQ1).

DOI: 10.1002/eqe

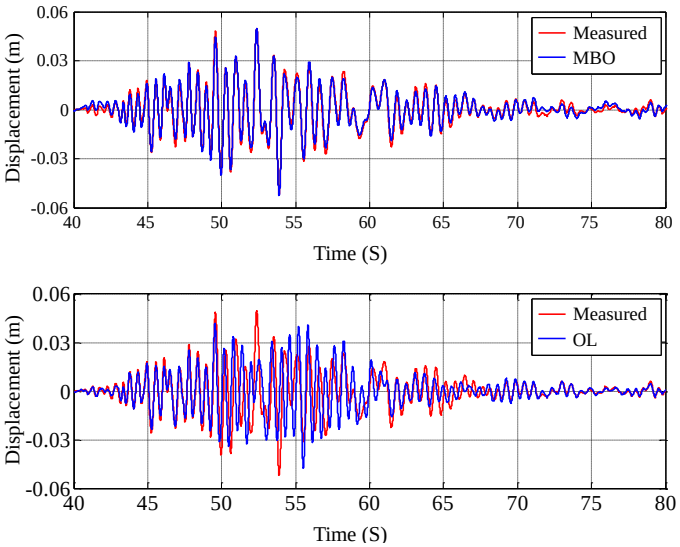

Figure 13. Displacement estimate at seventh story (EQ1).

The estimate of the relative acceleration (with respect to the base) at the sixth story is shown in Figure 12. As it can be seen, the MBO estimates are in agreement with the measured response. The figure in the lower panel shows the open-loop estimate ("OL"), i.e., the result from applying the base motion history to the reference finite element model, without using measurement feedback.

As can be seen, measurement feedback significantly improves the open-loop estimate, which is largely affected by modeling errors. The estimate of the lateral displacement at the top of the structure is shown in Figure 13. The estimate is in good agreement with the measured displacement. The estimates of the weight normalized base shear and overturning moment are depicted in Figure 14 and Figure 15 respectively. The weight of the structure is approximately $2000kN$.

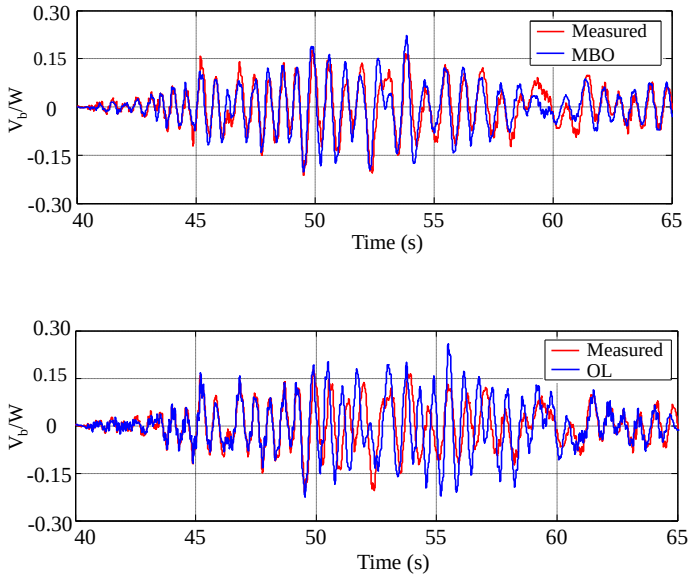

Figure 14. Estimate of the weight normalized base shear (EQ1).

DOI: 10.1002/eqe

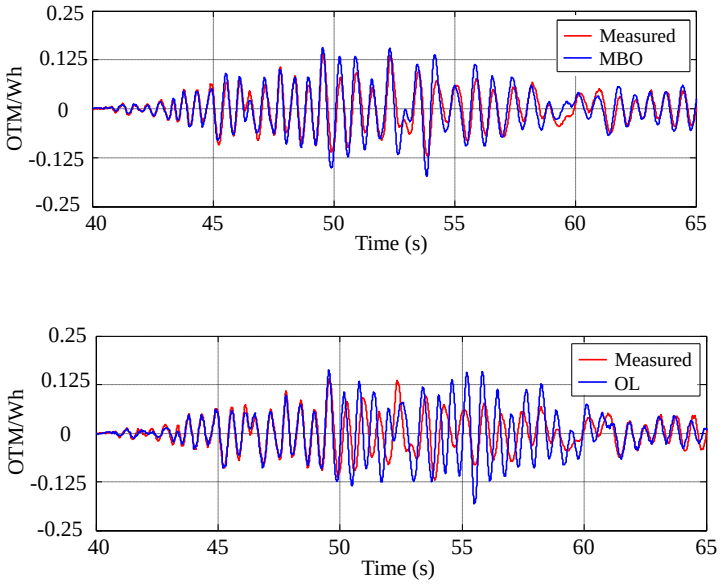

Figure 15. Overturning moment estimate (EQ1).

The estimates of the strain history at locations D1-2 and D2-2 are shown in Figure 16 (the LVDT layout is shown in Figure 4). The asymmetry in the measured response (i.e., larger positive than negative amplitude cycles) can be attributed to the fact that when this test was performed the structure had degraded significantly. Thus, the deformation when the LVDT is in tension is larger than the deformation when it is in compression due to crack opening. Based on system identification results, a reduction of 20% in the vibration frequency of the first mode of vibration was observed with respect to the initial "uncracked" state.

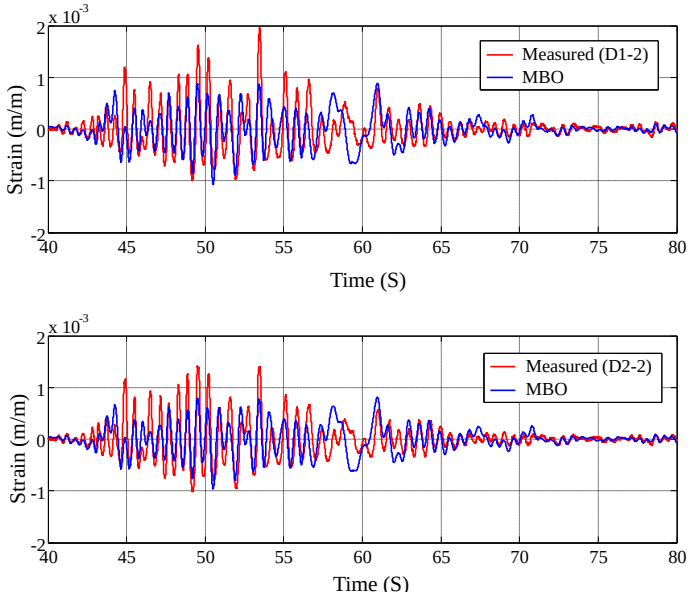

Figure 16. Strain estimates at locations D1-1 and D1-2 (EQ1).

DOI: 10.1002/eqe

To quantify the accuracy of the estimates the following metric was defined

$$\epsilon = \frac{\|x_m - \hat{x}\|_2}{\|x_m\|_2} \tag{13}$$

where x_m is the measurement of the quantity of interest x, $\hat{x}$ is the estimate of x, and $\|\|_2$ denotes the L_2 norm. Table III summarizes the results of the metric for the estimated quantities.

Table III. Error metric ϵ for EQ1 case.

	MBO	OL
Acceleration 3^{rd} story	0.57	1.34
Acceleration 5^{th} story	0.43	1.25
Acceleration 6^{th} story	0.39	1.29
Lateral displacement 7^{th} story	0.17	0.32
Strain D1-2	0.95	2.37
Strain D2-2	0.97	2.46
Base shear	0.29	0.51
Overturning moment	0.22	0.43

4.4.3. Moderate Amplitude Earthquake Input (EQ2) The third test studied corresponds to a moderate amplitude base motion. The applied input was the VNUY transverse component of the 1971 San Fernando earthquake (PGA=0.26g), denoted as "EQ2". The input base motion corresponds to test no. 91 according to the testing history [11]. The acceleration response at the foundation level and the magnitude of its Fourier spectra are shown, respectively, in the top and bottom panels of Figure 17. The measurements were sampled at 240Hz, detrended and band-passed (0.5-50Hz) using a high order 1024 FIR filter.

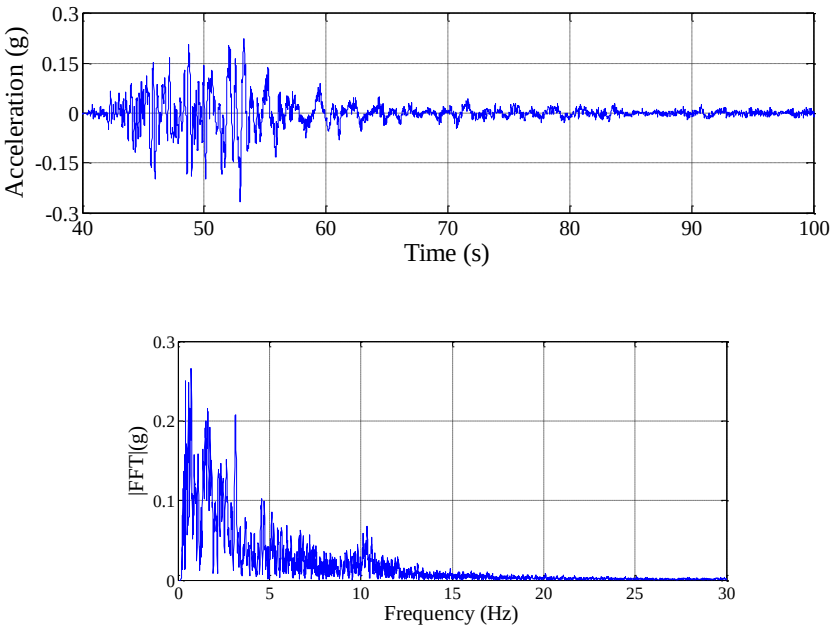

Figure 17. Moderate Amplitude Earthquake Input (EQ2) - VNUY transverse component of 1971 San Fernando earthquake (PGA=0.26g). Top: Time History. Bottom: Fourier Spectra amplitude.

DOI: 10.1002/eqe

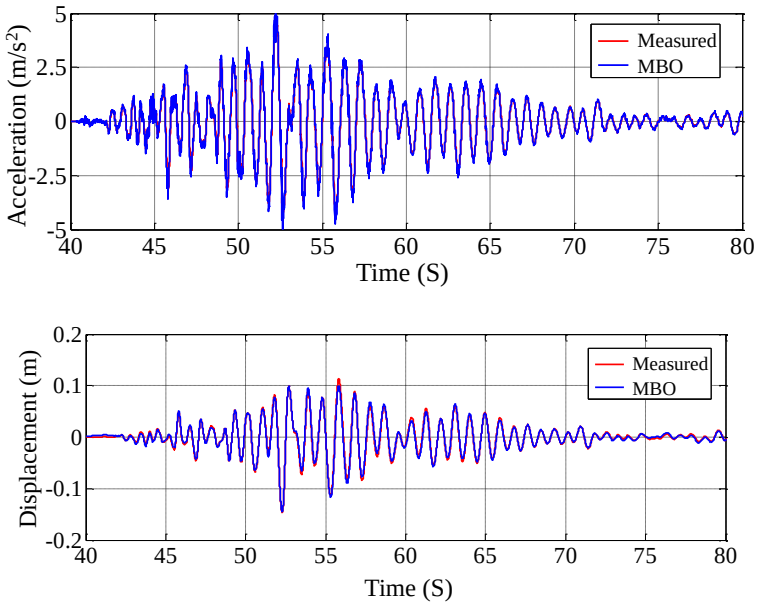

Figure 18. Top: Acceleration estimate at sixth story (EQ2). Bottom: Displacement estimate at seventh story (EQ2).

The MBO was implemented using the same parameters defined for the EQ1 case. The estimate of the relative acceleration (with respect to the base) at the sixth story and the displacement of the seventh floor are shown in Figure 18. Both estimates are in good agreement with the measured response. The estimates of the weight normalized base shear and overturning for the EQ2 case are shown in Figure 19,

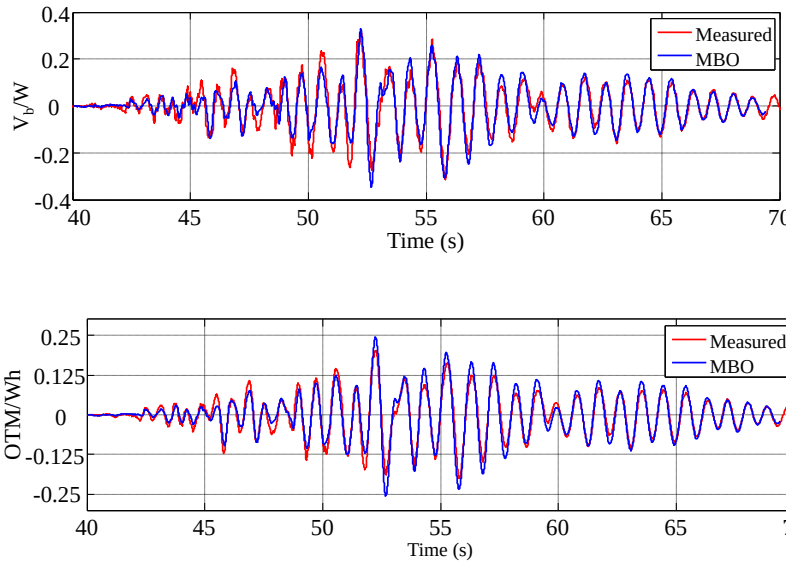

Figure 19. Base shear and overturning moment estimates (EQ2).

DOI: 10.1002/eqe

The strain estimates at locations D1-2 and D1-15 are shown in Figure 20. As can be seen, the crack opening effect is more pronounced in the measurement of strain D1-2, at the bottom of the first story wall. This phenomenon is not captured by the MBO estimate since the finite element model employed does not account for crack opening. Despite this limitation the estimates of the QoI are in good agreement with the measurements used for validation.

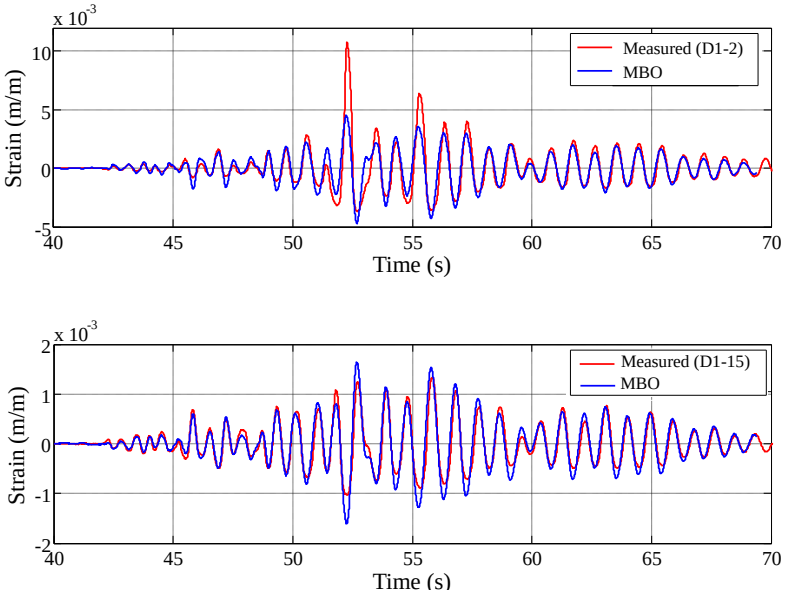

Figure 20. Strain estimates at locations D1-2 and D1-15 (EQ2).

5. CONCLUSIONS

This paper proposes the use of a model-based observer (MBO) to perform high-resolution seismic response estimation in partially instrumented building structures. The observer was employed to estimate the time history of quantities of interest (QoI) in earthquake engineering applications, such as lateral displacements, accelerations, strains at critical locations, base shear and overturning moment.

A numerical verification was conducted in the context of a five degree-of-freedom nonlinear shear model subjected to a moderate amplitude simulated support motion. Estimates obtained by implementing the proposed observer were found to be in close agreement with the nominal system response.

The proposed MBO was validated using data from a full-scale experiment carried out by an independent team of researchers from the University of California at San Diego. The experiment, conducted in the NEES-UCSD shake table, consisted of a seven story shear wall structure resembling a slice of a typical shear wall building. The data from the experiment is available to the research community through the NEES project warehouse website.

Measurements from three tests were used to validate the observer: a banded white noise input, and low/moderate amplitude records from the 1971 San Fernando earthquake. In all cases the observer was capable of estimating the QoI successfully, although a slight decrease in accuracy was noted as the base motion intensity was increased during the second and third tests, specially when estimating peak strain response. The simulated and experimental results presented in this paper indicate that the proposed observer is a promising algorithm to perform high-resolution estimation in partially instrumented building structures during earthquakes. Future work will focus on: a) improving the

DOI: 10.1002/eqe

estimation accuracy in cases of moderate and highly nonlinear response; and b) implementing the MBO in real buildings.

ACKNOWLEDGEMENT

This study was partially supported by the National Science Foundation awards ECC-1342190 and CMMI-1453502. NSF support is gratefully acknowledged.

The authors acknowledge the access to the "Shake Table Response of Full Scale Reinforced Concrete Wall Building Slice" (DOI:10.4231/D35T3G04T) project database of the NEES Project Warehouse (`https://nees.org/warehouse/experiment/295/project/203`), which is available to the research community under the ODC Attribution License (`http://opendatacommons.org/licenses/by/1.0/`). Access to the database is gratefully acknowledged.

REFERENCES

1. Beck J. Determining models of structures from earthquake records. *PhD Dissertation, California Institute of Technology* 1979; .
2. Betti. Identification of linear structural systems using earthquake-induced vibration. *Journal of Earthquake Engineering and Structural Dynamics* 1999; **28**(11):1449–1467.
3. De la Llera J, Chopra A. Evaluation of seismic code provisions using strong-motion building records from the 1994 northridge earthquake. *SMIP95 Seminar on Seismological and Engineering Implications of Recent Strong Motion Data* 1995; :25–40.
4. Bernal D, Hernandez E. A data driven methodology for assessing impact of earthquakes on the health of building structural systems. *Journal of Structural Design of Tall Buildings* 2006; **15**:21–34.
5. Naeim F. Real-time damage detection and performance evaluation for buildings. *Earthquakes and health monitoring of civil structures, Springer Environmental Science and Engineering* 2013; :167–196.
6. Erazo K, Hernandez E. Bayesian model-data fusion for mechanistic postearthquake damage assessment of building structures. *Journal of Engineering Mechanics* 2016; **10.1061/(ASCE)EM.1943-7889.0001114**:04016 062.
7. Mau T, Aruna V. Story-drift, shear and otm estimation from building seismic records. *Journal of Structural Engineering* 1994; **120**(11):3366–3385.
8. Limongelli M. Optimal location of sensors for reconstruction of seismic responses through spline function interpolation. *Earthq Eng Struct Dyn* 2003; **32**(1):1055–1074.
9. Hernandez E, Bernal D. State estimation in structural systems with model uncertainties. *Journal of Engineering Mechanics* 2008; **134**:252–257.
10. Hernandez E. A natural observer for optimal state estimation in second order linear structural systems. *Mech Syst Signal Process* 2011; **25**:2938–2947.
11. Panagiotou M, Restrepo J, Conte J. Shake table response of 7-story rc bearing wall building. *Network for Earthquake Engineering Simulation (distributor), Dataset, DOI:10.4231/D35T3G04T* 2013; .
12. Moaveni B, He X, Conte J, Restrepo J. Damage identification study of a seven-story full-scale building slice tested on the ucsd-nees shake table. *Structural Safety* 2010; (32):347–356.
13. Moaveni B, He X, Conte J, Restrepo J, Panagiotou M. System identification study of a seven-story full-scale building slice tested on the ucsd-nees shake table. *Journal of Structural Engineering* 2011; **137**(6):705–717.
14. Luenberger D. *Observer Theory*. John Wiley and Sons: New York, NY, USA, 1970.
15. Brogan W. *Modern Control Theory*. Prentice Hall: New Jersey, USA, 1991.
16. Waller H, Schmidt R. The application of state observers in structural dynamics. *Mechanical Systems and Signal Processing* 1990; **4**(3):195–213.
17. Ching J, Beck J, Porter K, Shaikhutdinov R. Bayesian state estimation method for nonlinear systems and its application to recorded seismic response. *Journal of Engineering Mechanics* 2006; **132**:396–410.
18. Erazo K, Hernandez E. Uncertainty quantification of state estimation in nonlinear structural systems with application to seismic response in buildings. *ASCE/ASME Journal of Risk and Uncertainty in Engineering Systems* 2015; **B5015001**.
19. Erazo K, Hernandez E. A model-based observer for state and stress estimation in structural and mechanical systems: Experimental validation. *Mechanical Systems and Signal Processing* 2014; **43**:141–152.
20. Bouc R. Modele mathematique d'hysteresis. *Acustica* 1971; **24**:16–25.
21. Wen Y. Method for random vibration of hysteretic systems. *Journal of Engineering Mechanics* 1976; **102**:249–263.
22. Ortiz G, Alvarez D, Bedoya-Ruiz D. Identification of Bouc Wen type models using multi-objective opimization algorithms. *Computers and Structures* 2013; (114-115):121–132.
23. Thrainsson H, Kiremidjian A, Winterstein S. Modeling of earthquake ground motion in the frequency domain. *The John A. Blume Earthquake Engineering Center, Stanford University* 2000; **Report No.134**.
24. Pires J, Wen Y, Ang A. Stochastic analysis of liquefaction under earthquake loading. *Civil Engineering Studies, UIUC* 1983; .
25. Vanmarcke E, Lai SSP. Strong motion duration and rms amplitude of earthquake records. *Bulletin of the Seismological Society of America* 1980; **70**(4):1293–1307.
26. Iyengar R, Iyengar K. A nonstationary random process model for earthquake accelerograms. *Bulletin of the Seismological Society of America* 1969; **59**(3):1163–1188.
27. Panagiotou M, Restrepo J, Conte J. Shake table test of a 7-story full scale reinforced concrete structural wall building slice phase i: Rectangular wall section. *UCSD Report No. SSRP-07-07* 2007; .

28. Priestley M, Kowalsky M. Direct displacement-based seismic design of concrete buildings. *Bulletin of the New Zealand National Society for Earthquake Engineering* 2000; **33**(4):421–444.
29. Computers, Structures I. *SAP2000, V17.1*. 2014.
30. Khan F, Sbarounis J. Interaction of shear walls and frames. *Journal of the Structural Division* 1964; **90**(3):285–335.
31. Park Y, Ang A, Wen Y. Seismic damage analysis and damage-limiting design of r.c. buildings. *Technical Report of Research, Civil Engineering Studies No. 516, UIUC* 1984; .
32. Miranda E. Approximate seismic lateral deformation demands in multistory buildings. *Journal of Structural Engineering* 1999; **125**:417–425.
33. Blume J. Dynamic characteristics of multi-story buildings. *ASCE Journal of the Structural Division* 1968; **94**:337–402.
34. Chopra A, Cruz E. Evaluation of building code formulas for earthquake forces. *ASCE Journal of Structural Engineering* 1986; **112**:1881–1899.
35. Uang C, Maarouf A. Safety and economy considerations of ubc seismic force reduction factors. *Proc. 1993 Nat. Conf., Central United States Earthquake Consortium, Memphis* 1993; :121–130.
36. Lutes L, Sarkani S. *Random Vibrations: Analysis of Structural and Mechanical Systems*. Elsevier, 2004.
37. Kanai K. Semi-empirical formula for the seismic characteristics of the ground. *Bull. Earthq. Res. Inst., University of Tokyo* 1957; **35**.
38. Tajimi H. Statistical method of determining the maximum response of building structure during an earthquake. *Proc. of the 2nd WCEE 2* 1960; :781–798.

DOI: 10.1002/eqe